An actomyosin-polarized membrane reservoir mediates the unequal divisions of *Drosophila* neural stem cells

Bryce LaFoya and Kenneth E. Prehoda

Institute of Molecular Biology
Department of Chemistry and Biochemistry
1229 University of Oregon
Eugene, OR 97403

Corresponding author: prehoda@uoregon.edu

Summary

The asymmetric divisions of *Drosophila* neural stem cells (NSCs) produce unequally sized siblings, with most volume directed into the sibling that retains the NSC fate. Sibling size asymmetry results from preferential expansion of the NSC sibling surface during division. Here we show that a polarized membrane reservoir constructed by the NSC in early mitosis provides the source for expansion. The reservoir is formed from membrane domains that contain folds and microvilli that become polarized by apically-directed cortical flows of actomyosin early in mitosis. When furrow ingression begins and internal pressure increases, the stores of membrane within the apical reservoir are rapidly consumed. Expansion is significantly diminished in NSCs that lack a reservoir, and membrane expansion equalizes when the reservoir is not polarized. Our results suggest that the cortical flows that remodel the plasma membrane during asymmetric cell division function to satisfy the dynamic surface area requirements of unequally dividing cells.

Introduction

Cellular resources can be partitioned unequally during division to facilitate differences in sibling cell fate and proliferation potential. For example, dividing *Drosophila* neural stem cells (NSCs) direct most cell volume into the sibling that retains the NSC fate and remains highly proliferative. In contrast, the neural precursor (NP) sibling that is destined towards differentiation and a postmitotic state receives a small fraction of the total volume (Gallaud et al., 2017; Homem and Knoblich, 2012). While asymmetric spindle positioning can contribute to unequal cell division, the size asymmetry of the NSC and NP cells results from preferential expansion of the NSC sibling during anaphase (Cabernard et al., 2010; Connell et al., 2011; Pham et al., 2019; Roubinet et al., 2017). Biased expansion is characterized by a rapid increase in surface area near the NSC pole while the area near the other pole remains relatively constant (Connell et al., 2011). Expansion occurs when intracellular hydrostatic pressure increases following the initiation of furrow ingression (Pham et al., 2019). While a biased increase in surface area is a key aspect of the unequal NSC division, little is known about how the plasma membrane accommodates asymmetric polar expansion. Here we examine the plasma membrane dynamics that support the geometric changes that accompany the unequal NSC division.

Cell shape changes can significantly alter surface area, placing significant demands on the plasma membrane. Many animal cells, including the *Drosophila* NSC, round up during division

33 to assume a geometry that uses surface area most efficiently for a given volume. The surface
34 area can increase when the NSC deviates from sphericity as it elongates and expands, like a
35 pinched balloon. However, the plasma membrane is relatively inelastic and can only undergo
36 limited stretching to accommodate increases in surface area. One mechanism that cells use to
37 buffer changes in surface area is to store membrane in cell surface reservoirs (Figard et al.,
38 2013; Figard and Sokac, 2014; Kabeche et al., 2015). Membrane reservoirs use folds and
39 microvilli to store membrane that is unnecessary for encapsulating the cell (i.e. excess
40 membrane). When shape changes decrease surface area, excess membrane can be rapidly
41 stored in these structures. Conversely, increases in surface area can potentially be rapidly
42 accommodated by tapping into the reservoir, reducing the amount of excess membrane.

43 The NSC is not known to store membrane in reservoirs. However, the NSC membrane
44 undergoes a polarity cycle that resembles its well-characterized protein polarity cycle (LaFoya
45 and Prehoda, 2021). During the protein cycle, polarity proteins and fate determinants become
46 polarized to the NSC's apical and basal hemispheres during early mitosis (Gallaud et al., 2017;
47 Homem and Knoblich, 2012; Knoblich, 2010, 2008). The apical proteins are polarized in part by
48 apically-directed cortical flows of actomyosin. These cortical movements lead to the formation
49 of an organized cap near the apical pole that remains until it depolarizes shortly before division
50 (Oon and Prehoda, 2021, 2019). The plasma membrane undergoes a similar cycle in which
51 membrane features that are initially dispersed over the surface of the cell move apically, in
52 synchrony with polarity proteins, before appearing to spread over the surface by moving
53 basally during anaphase. The dynamic NSC membrane features can be detected with diverse
54 membrane sensors and some are clearly microvilli suggesting that they could store excess
55 membrane. Here we examine whether the NSC membrane contains a reservoir and if so, how
56 membrane dynamics might contribute to the biased expansion that mediates unequal NSC
57 division.

58 **Results**

59 **The apparent surface area of the apical NSC sibling increases during division**

60 To estimate the potential demand for plasma membrane during NSC division, we measured the
61 expansion of cellular surface area from metaphase to the completion of cytokinesis in
62 *Drosophila* larval brain NSCs (Figure 1A,B). We compared the *apparent* total surface area at
63 both time points, where the apparent surface area refers to that of the main cell body exclusive
64 of surface area contained in folds or microvilli (Figure 1C). We measured an average surface

65 area increase of 63 ± 22 μm^2 (n = 10), which was approximately equal to half the apparent
66 surface area of the NP cell on average (118 ± 12 μm^2; n = 10) (Figure 1D). Expansion during
67 NSC division is biased, such that most expansion occurs near the apical pole (Connell et al.,
68 2011; Pham et al., 2019; Roubinet et al., 2017). We conclude that the NSC division creates a
69 demand for new surface area that is apparently satisfied by a biased expansion process that
70 directs the increase in surface area towards the apical pole.

71 **Neural stem cell membrane domains store excess membrane**

72 We sought to understand how the plasma membrane supports the increase in apparent
73 surface area of the NSC's apical region during division. The NSC membrane is heterogeneous,
74 with distinct domains characterized by localized areas of relatively high membrane sensor
75 intensity (Figure 1E) (LaFoya and Prehoda, 2021). NSC membrane domains are distributed
76 across the cell surface in interphase and early mitosis and can be detected with diverse
77 membrane sensors. The higher sensor intensity within NSC membrane domains could arise
78 from an increased density of specific membrane components in a single bilayer (Figure 1F-
79 scheme 1). Alternately, however, increased amounts of plasma membrane in the form of folds
80 or microvilli could also lead to higher sensor intensity (Figure 1F-scheme 2), and some microvilli
81 are known to be present (LaFoya and Prehoda, 2021). We term the fine structure of the
82 membrane in folds and microvilli, "excess membrane", as it extends away from the cell surface
83 and therefore appears to be unnecessary for encapsulating the NSC. We examined the
84 prevalence of excess membrane by measuring the thickness of domains in early mitosis when
85 the NSC is rounded up using super resolution imaging (Azuma and Kei, 2015). NSC membrane
86 domains were nearly exclusively associated with increased thickness relative to surrounding
87 areas, which had a relatively uniform thickness approximately equal to the diffraction limited
88 width (Figure 1G). We conclude that excess membrane is stored on the NSC surface in
89 discrete regions that are thicker than surrounding regions and often contain microvilli. The
90 presence of excess membrane makes the total NSC membrane surface area greater than the
91 apparent surface area of the cell body, a phenomenon that has been compared to the
92 "coastline paradox" in which the size of an interface is influenced by the presence of structure
93 at different length scales (Sokac, 2017).

94 **Excess plasma membrane moves apically to form a polarized membrane reservoir**

95 NSC membrane domains that are dispersed over the cell surface in early mitosis become
96 concentrated around the apical pole by metaphase (Figure 2A and Video S1) (LaFoya and

97 Prehoda, 2021). Given our finding that membrane domains store excess membrane, we
98 hypothesized that the polarization process causes excess membrane to accumulate near the
99 apical pole. Consistent with this hypothesis, we measured a significant increase in apical
100 membrane thickness at metaphase compared to prophase (Figure 2B,C). We did not detect
101 any basally-directed movement of excess membrane during this time period. We also
102 observed deformation of domains along the apical-basal axis as they moved towards the
103 apical pole (c.f. Figure 2A inset, Video S1), suggesting the presence of tension-induced
104 stretching. We conclude that the polarization of the NSC membrane occurs at least in part from
105 accumulation of excess membrane around the apical pole due to its directional transport from
106 around the cell surface.

107 **Cortical actomyosin flows drive apical plasma membrane accumulation**

108 The apically-directed membrane domain movements that construct the polarized membrane
109 reservoir do not occur in Latrunculin A-treated NSCs (LaFoya and Prehoda, 2021), indicating
110 that they require F-actin. The requirement of F-actin, along with the recent discovery of
111 apically-directed cortical flows of actomyosin in prophase NSCs (Oon and Prehoda, 2021),
112 suggest that cortical flows could drive the formation of the apical membrane reservoir. We
113 examined whether cortical cytoskeletal flows are correlated with membrane polarization
114 dynamics using simultaneous imaging of the membrane and F-actin. As previously reported
115 (LaFoya and Prehoda, 2021), we observed enrichment of F-actin at sites of excess membrane
116 (Figure 3 and Video S2). Here we find that the movements that polarize membrane domains are
117 highly correlated with cortical F-actin dynamics (Figure 3B and Video S2). Cortical F-actin has
118 been reported to become enriched near the apical pole at metaphase (Oon and Prehoda, 2021;
119 Roubinet et al., 2017), and our results suggest that F-actin enrichment is the result of its
120 presence in the apically-polarized membrane domains. The correlated motions of actin and
121 membrane, along with the requirement of F-actin for these movements, suggest that cortical
122 flows of actin are responsible for constructing the apical membrane reservoir.

123 **The apical membrane reservoir is consumed during NSC division**

124 Our data indicate that the NSC constructs a polarized membrane reservoir in early mitosis by
125 moving excess membrane to the apical pole using actomyosin driven cortical flows. We
126 examined whether the apical membrane reservoir is consumed during anaphase, when the
127 apical region's apparent surface area increases (Connell et al., 2011; Pham et al., 2019). The
128 internal pressure of the NSC changes dramatically during this phase of the cell cycle, peaking

129 shortly after furrow ingression followed by a rapid decrease that coincides with membrane
130 expansion (Pham et al., 2019). We followed the dynamics of the apical membrane reservoir
131 during anaphase using super resolution imaging with high temporal resolution. We observed
132 thinning of the apical membrane that coincided with the broad equatorial narrowing associated
133 with the start of cytokinesis and the increase in apical surface area (Figure 4 and Video S3, S4;
134 reservoir formation and consumption are shown in Video S4). Microvilli that extended over a
135 micron from the cell surface were reabsorbed into the cell as furrowing continued (Figure 4A-
136 inset and Video S3, S4). The reservoir was consumed locally in smaller domains rather than
137 uniformly across the apical surface, suggesting that mechanical failure points may exist that
138 begin to unfold once the pressure reaches a certain threshold. As membrane reservoir
139 consumption occurred, the apical surface expanded and the remaining domains of excess
140 membrane appeared to move basally, as previously reported (LaFoya and Prehoda, 2021). As
141 apical expansion occurred, F-actin formed puncta that spread over the surface (Figure 5 and
142 Video S5). Thus, NSCs construct a polarized membrane reservoir in early metaphase that is
143 consumed during furrow ingression as the apical membrane expands.

144 **The membrane reservoir is required for expansion and completion of cytokinesis**

145 Our data indicate that the apical membrane reservoir is consumed during anaphase,
146 suggesting that the reservoir mediates preferential expansion at the apical pole. To investigate
147 how the NSC division process proceeds without a reservoir, we examined the divisions of
148 cyclodextrin-treated NSCs. Cyclodextrin treatment can ablate membrane domains in diverse
149 cell types (Barman and Nayak, 2007; Pang et al., 2007), perhaps because it extracts
150 cholesterol, significantly decreasing membrane rigidity (Chakraborty et al., 2020). In previous
151 work, we found that cyclodextrin treatment inhibits formation of NSC membrane features
152 (LaFoya and Prehoda, 2021). Consistent with previous observations, we found that the
153 membranes of cyclodextrin-treated NSCs were relatively featureless such that the plasma
154 membrane smoothly followed the contours of the cell (Figure 6A), apparently lacking any
155 excess membrane. In the absence of a membrane reservoir, very little polar expansion
156 occurred, and furrowing was incomplete and unstable (Figure 6B,C and Video S6). These
157 results suggest that expansion requires a membrane reservoir. Furthermore, reservoir-
158 mediated expansion may provide a “pressure relief valve” that prevents the intracellular
159 pressure from continuing to increase as the furrow ingresses. The increase in intracellular
160 hydrostatic pressure that coincides with the onset of furrow ingression (Pham et al., 2019), may

161 be released by membrane reservoir-mediated expansion and without a reservoir, intracellular
162 pressure may increase to the point where the furrow is no longer able to ingress.

163 **Membrane reservoir polarization is required for biased expansion**

164 Our data suggest that membrane reservoir polarization mediates biased expansion during NSC
165 division. We examined how failure to polarize the membrane reservoir influences expansion
166 using NSCs expressing RNAi directed against the heterotrimeric G-protein Gγ1 (hereafter Gγ).
167 Gγ is known to be required for asymmetric NSC division (Izumi et al., 2004), and we found that
168 NSCs expressing Gγ RNAi do not polarize their membranes in early mitosis (Figure 7 and Video
169 S7). Like wild-type NSCs, cells expressing Gγ RNAi had excess membrane distributed over the
170 cell surface in early mitosis. However, the apically-directed movements that polarize the
171 membrane reservoir of wild-type NSCs failed to occur in Gγ RNAi-expressing cells. Without
172 these polarizing movements, these cells failed to form a membrane reservoir at the apical pole
173 as excess membrane remained distributed across the cell surface as furrow ingression
174 commenced (Figure 7B,C). In the absence of a polarized membrane reservoir, the expansion
175 that occurred following ingression was equally distributed to both poles and daughter cell size
176 was approximately symmetric. We conclude that the biased expansion of the NSC membrane
177 is mediated by polarization of the membrane reservoir before division.

178 **Discussion**

179 The morphological changes that accompany cell division can place significant demands on the
180 plasma membrane by rapidly increasing total surface area. During the unequal divisions of
181 *Drosophila* NSCs, the surface area increase is biased, with the nascent NSC surface expanding
182 as the furrow ingresses while the NP surface remains relatively constant (Connell et al., 2011;
183 Pham et al., 2019). In general, the demand for membrane can be buffered by reservoirs of
184 excess membrane stored in folds and microvilli, or eisosomes in yeast (Figard et al., 2016;
185 Figard and Sokac, 2014; Goudarzi et al., 2017; Kabeche et al., 2015). We discovered a
186 membrane reservoir that mediates the biased expansion that occurs during NSC asymmetric
187 division (Figure 7D). The reservoir is constructed from localized regions of excess membrane
188 that are dynamically collected at the apical pole by apically-directed cortical flows of
189 actomyosin that begin and end in early mitosis (Oon and Prehoda, 2021). When expansion
190 begins following the initiation of cleavage furrow ingression, the excess membrane in the
191 reservoir is consumed, coinciding with a rapid drop in internal hydrostatic pressure that occurs
192 during anaphase (Pham et al., 2019). In addition to explaining the source of membrane for

193 biased NSC expansion, these results have implications for the function of the complex cortical
194 actomyosin dynamic phases that occur during NSC asymmetric division. Furthermore, they
195 raise questions about how cortical actomyosin dynamics are coupled to the organization of the
196 NSC membrane, and how intracellular pressure and actomyosin dynamics are coupled to
197 expansion-induced tapping of the reservoir. Polarized membrane structures have also been
198 reported in the asymmetrically-dividing *C. elegans* zygote (Hirani et al., 2019; Scholze et al.,
199 2018), suggesting that they may play a more general role in asymmetric division.

200 Examination of NSC membrane dynamics revealed that the cell goes to great lengths to
201 prepare for biased expansion, generating directional cortical flows to collect excess membrane
202 at the apical pole (Figure 2). Directional cortical flows of actomyosin play a role in the
203 polarization of both the plasma membrane and proteins during the NSC division (LaFoya and
204 Prehoda, 2021; Oon and Prehoda, 2021, 2019), and their role in cortical protein polarity of the
205 *C. elegans* zygote has been extensively studied (Illukkumbura et al., 2019; Lang and Munro,
206 2017; Munro et al., 2004). While cortical movements of polarity proteins such as aPKC are
207 driven by actomyosin cortical flows in the NSC, F-actin is not strictly required for its polarity.
208 For example, in Latrunculin A treated NSCs that lack an actin cytoskeleton, aPKC polarizes but
209 ultimately diffuses into the basal hemisphere (Oon and Prehoda, 2019). Thus, currently
210 available data suggest that actomyosin cortical flows in the NSC function primarily to organize
211 the membrane and are not essential for establishing protein polarity, even while the cortical
212 cytoskeleton maintains protein polarity by preventing spreading into the basal hemisphere
213 (LaFoya and Prehoda, 2021; Oon and Prehoda, 2019).

214 Localized regions of excess membrane move to the apical pole during prophase to generate
215 the NSC membrane reservoir. How might actomyosin-generated cortical flows be coupled to
216 the directional movement of excess membrane domains? In cultured mammalian epithelial
217 cells, microvilli move rapidly across the cell surface to form the brush border (Meenderink et
218 al., 2019). In this context, microvillar motion has been proposed to be driven by treadmilling of
219 an interior actin bundle. In the NSC, apically-directed cortical flows of actomyosin not only
220 move excess membrane but deform the surrounding tissue (LaFoya and Prehoda, 2021; Oon
221 and Prehoda, 2021), suggesting that the flows are coupled to a broad range of membrane-
222 associated structures, including adhesions. The deformations of excess membrane domains
223 along the apical-basal axis suggest that tension in the membrane is generated as the domains
224 are gathered at the apical pole.

The apical reservoir is tapped shortly after its creation in metaphase (Figure 4), coinciding with the onset of furrow ingression and the peak of internal hydrostatic pressure (Pham et al., 2019). Simultaneously with these processes, myosin II redistributes from the apical pole towards the cleavage furrow (Oon and Prehoda, 2021; Pham et al., 2019; Roubinet et al., 2017). Reservoir consumption could be caused by myosin relocalization or the initiation of furrow ingression, or a combination of both processes. Alternately redistribution of myosin could be a mechanical consequence of reservoir tapping. Future work will be directed at understanding the physical mechanisms that couple cortical actomyosin dynamics to membrane movements in the NSC, and the role these dynamics play in coupling reservoir consumption and cell surface expansion.

Acknowledgments

This work was supported by NIH grants GM127092 and F32GM134705.

Star Methods

Resource Availability

Lead Contact

Further information and requests for resources and reagents should be directed to the Lead Contact, Kenneth Prehoda (prehoda@uoregon.edu).

Materials Availability

This study did not generate new unique reagents.

Data and Code Availability

The raw data supporting the current study have not been deposited in a public repository because of their large file size, but are available from the corresponding author on request.

Experimental Model and Subject Details

Fly Strains

For tissue specific expression of UAS controlled transgenes in NSCs, a Worniu-Gal4 driver line was used. For live imaging of membrane dynamics, two different classes of membrane-bound fusion proteins were used, both of which nearly exclusively label the plasma membrane and

256 not internal membranes in NSCs. Farnesyl-GFP expresses the C-terminal region of human K-
257 Ras tagged with GFP which becomes farnesylated and plasma membrane-anchored in cells.
258 PH-GFP and PH-mCherry express the pleckstrin homology domain of human PLCδ tagged
259 with GFP or mCherry, which binds to the plasma membrane lipid phosphoinositide PI(4,5)P2.
260 Live imaging of actin dynamics was achieved using the F-actin marker Lifeact-mRuby
261 expressed in NSCs. Progression through mitosis was tracked by expressing the microtubule
262 marker Zeus-mCherry, which labels the mitotic spindle in NSCs. Symmetrical cell division in
263 NSCs was induced through the expression of dsRNAi of G protein γ1 (Gγ1, FBgn0004921)
264 under UAS control. Miranda-GFP expresses GFP tagged Miranda at the endogenous loci
265 (Ramat et al., 2017).
266
267 **Method Details**
268 ***Live Imaging***
269 Intact *Drosophila* central nervous systems were dissected from third instar larvae in a bath of
270 Schneider's Insect Media. These larval brain explants were then mounted dorsal side down on
271 sterile poly-D-lysine coated 35mm glass bottom dishes (ibidi Cat#81156) containing modified
272 minimal hemolymph-like solution (HL3.1). Explants were imaged on a Nikon Eclipse Ti-2 (60x
273 H_2O objective) equipped with a Yokogawa CSU-W1 SoRa spinning disk head and dual
274 Photometrics Prime BSI sCMOS cameras. GFP tagged proteins were illuminated with 488nm.
275 Proteins tagged with mCherry and mRuby were illuminated with 561nm laser light. For
276 standard resolution time lapse imaging a z-stack of 41-61 optical sections with a step size of
277 0.5 μm was acquired every 10 seconds. For super resolution imaging, individual NSCs were
278 imaged using SoRa optics which achieve super resolution through optical photon
279 reassignment. For time lapse super resolution imaging, images were acquired every 2-60
280 seconds. For z-stacks acquired during super resolution imaging, a step size of 0.3 μm was
281 used. Where time relative to anaphase onset is noted, anaphase onset was identified as the
282 frame in which the apical membrane begins its expansion which coincides with the separation
283 of the sister chromatids (LaFoya and Prehoda, 2021). To examine the effects of cyclodextrin on
284 membrane dynamics, explants were treated with 15 mM methyl-β-cyclodextrin (solubilized in
285 HL3.1) for 4 hours prior to imaging. To study cyclodextrin's effects on cytokinesis (Figure 6b),
286 NSCs expressing PH-GFP and Zeus-mCherry and incubated with methyl-β-

287 cyclodextrin (n=10) or left untreated (n=10) were imaged throughout mitosis and assessed on
288 their ability to complete cytokinesis or not.
289
290 ***Image Processing and Analysis***
291 Images were analyzed using ImageJ (FIJI package) and Imaris (Bitplane) software. NSCs were
292 identified through their location in the brain and large size, as well as the presence of
293 transgenes expressed from the NSC specific promoter Worniu. 3D projections were created by
294 z-stack processing in ImageJ, using the maximum intensity projection method for standard
295 resolution imaging and standard deviation projection method for super resolution imaging.
296 Only optical slices from the front hemisphere of the NSC were used to create 3D projections.
297 We define a medial optical slice as a single optical slice through the center of the cell along the
298 apical-basal axis. Photobleaching during time-lapse imaging was corrected for using ImageJ
299 bleach correction tool in histogram matching mode. When image deconvolution was applied,
300 deconvolution was performed using Nikon Elements standard 2D deconvolution mode. Image
301 deconvolution was applied to Video S3 NSCs #3, 7, & 8. Kymographs (Fig. 3b) were created
302 from time-lapse video using a line along the apical-basal axis using ImageJ multi kymograph
303 tool. To reduce image noise, Gaussian blur was applied to the Zeus-mCherry channel in Figure
304 6c using ImageJ.
305
306 For the cell surface area quantifications (Figure 1d), the surface area of cells marked with the
307 basal marker Miranda was determined using the following method. In ImageJ, a medial optical
308 slice was used to measure the diameter of the cell at five different angles. From the average
309 diameter of the cell, the surface area was calculated using the equation $SA = 4\pi r^2$, where SA =
310 surface area and r = radius. The surface area of the NSC at metaphase was compared to the
311 combined surface area of the NSC and its progeny cell just after they became separated
312 during division. The overall increase in apparent surface area that accompanies NSC division
313 was plotted for n=10 NSCs.
314
315 To quantify the thickness of membrane domains (Figure 1g), the thickness of the plasma
316 membrane within membrane domains and outside of membrane domains was determined
317 using the following method. NSCs were marked with two different membrane markers, Farnysl-
318 GFP and PH-mCherry. A membrane domain was identified as a region of the plasma
319 membrane which had high signal intensity in both channels, relative to other regions of the

320 plasma membrane. Medial optical slices from seven different NSCs were used to measure the
321 thickness of the plasma membrane within four distinct membrane domains and also at four
322 regions outside of membrane domains for each cell (totaling n=28 for each). Gardner-Altman
323 estimation plots for two group datasets and 95% confidence intervals of membrane thickness
324 were prepared using the DABEST package (Ho et al., 2019).
325
326 To quantify membrane thickness at the apical and basal poles (Figures 2b, 2c, 4c, 4d, 7b, and
327 7c) medial optical slices of NSCs were acquired using super resolution imaging. Images were
328 loaded into ImageJ, and a line which traversed the cell membrane at (or near to) either the
329 apical or basal pole was drawn. A plot profile was generated and the signal intensity peak
330 correlating to the cell membrane was identified based on its position and high intensity over
331 background signal. The length of the base of the peak was measured to determine the
332 thickness of the cell membrane. Measurements were taken at various stages of the cell cycle
333 and compared. When quantifying the effects of Gγ1 RNAi on membrane thickness the same
334 protocol was used, but only NSCs which divided symmetrically were quantified. Gardner-
335 Altman estimation plots for paired datasets and 95% confidence intervals of membrane
336 thickness were prepared using the DABEST package (Ho et al., 2019) for n=4 NSCs.
337
338 ***Quantification and Statistical Analysis***
339 Gardner-Altman estimation plots and 95% confidence intervals of datasets were prepared
340 using the DABEST package (Ho et al., 2019). Statistical details can be found in the relevant
341 methods section and figure legend.
342
343 **Key Resources Table**

REAGENT or RESOURCE	SOURCE	IDENTIFIER
Chemicals, Peptides, and Recombinant Proteins		
Methyl-β-cyclodextrin	Caymen Chemical	Cat#21633, CAS# 128446-36-6
Experimental Models: Organisms/Strains		
Farnesyl-GFP	Bloomington *Drosophila* Stock Center	BDSC Cat#80052, RRID:BDSC_80052
Lifeact-mRuby	Bloomington *Drosophila* Stock Center	BDSC Cat#35545, RRID:BDSC_35545

Miranda-GFP	Jens Januschke Lab	
PH-GFP	Bloomington *Drosophila* Stock Center	BDSC Cat#39693, RRID:BDSC_39693
PH-mCherry	Bloomington *Drosophila* Stock Center	BDSC Cat#51658, RRID:BDSC_51658
Worniu-Gal4	Chris Q. Doe Lab	
Zeus-mCherry	Chris Q. Doe Lab	
Gγ1 RNAi	Bloomington *Drosophila* Stock Center	BDSC Cat#34372, RRID:BDSC_34372
Software and Algorithms		
ImageJ (FIJI package)	National Institutes of Health	
Imaris	Bitplane	
Elements	Nikon	

346 **Video Legends**

347 Video S1: NSC membrane dynamics in early mitosis that lead to reservoir formation
348 Super resolution videos of PLCδ-PH-GFP (worniu-GAL4>UAS- PLCδ-PH-GFP; "PH-GFP")
349 expressing NSCs in early mitosis shown in standard deviation projections and in medial
350 sections.

351 Video S2: Correlated NSC membrane and cortical actin dynamics in early mitosis
352 Standard resolution videos of PLCδ-PH-GFP (worniu-GAL4>UAS- PLCδ-PH-GFP; "PH-GFP")
353 and cortical F-actin (worniu-GAL4>UAS-Lifeact-mRuby; "Lifeact") expressing NSCs in early
354 mitosis shown in maximum intensity projections and in medial sections.

355 Video S3: NSC membrane dynamics during anaphase expansion
356 Super resolution videos of PLCδ-PH-GFP ("PH-GFP") expressing NSCs during anaphase
357 shown in standard deviation projections and in medial sections. Image deconvolution was
358 applied to NSCs #3, 7, & 8.

359 Video S4: NSC membrane dynamics during mitosis
360 Super resolution videos of PLCδ-PH-GFP (worniu-GAL4>UAS- PLCδ-PH-GFP; "PH-GFP")
361 expressing NSCs showing complete mitosis in standard deviation projections and in medial
362 sections.

363 Video S5: Correlated NSC membrane and cortical actin dynamics during anaphase expansion
364 Super resolution videos of PLCδ-PH-GFP (worniu-GAL4>UAS- PLCδ-PH-GFP; "PH-GFP") and
365 cortical F-actin (worniu-GAL4>UAS-Lifeact-mRuby; "Lifeact") expressing NSCs in early mitosis
366 shown in standard deviation projections and in medial sections.

367 Video S6: Membrane dynamics in cyclodextrin-treated NSCs
368 Super resolution videos of PLCδ-PH-GFP (worniu-GAL4>UAS- PLCδ-PH-GFP; "PH-GFP") and
369 microtubules (worniu-GAL4>UAS-Zeus-mCherry; "Zeus-mCherry") expressing NSCs treated
370 with cyclodextrin (NSCs #1-4) or untreated (NSC #5) shown in medial sections.

371 Video S7: Membrane dynamics in Gγ RNAi expressing NSCs
372 Super resolution (NSC #1) and standard resolution (NSCs #2 & 3) videos of PLCδ-PH-GFP
373 (worniu-GAL4>UAS- PLCδ-PH-GFP; "PH-GFP") and Gγ RNAi (worniu-GAL4>UAS- Gγ RNAi)
374 expressing NSCs shown in 3D projections and in medial sections.

375 **References**

376 Azuma T, Kei T. 2015. Super-resolution spinning-disk confocal microscopy using optical
377 photon reassignment. *Opt Express* **23**:15003–15011. doi:10.1364/OE.23.015003
378 Barman S, Nayak DP. 2007. Lipid raft disruption by cholesterol depletion enhances influenza A
379 virus budding from MDCK cells. *J Virol* **81**:12169–12178. doi:10.1128/JVI.00835-07
380 Cabernard C, Prehoda KE, Doe CQ. 2010. A spindle-independent cleavage furrow positioning
381 pathway. *Nature* **467**:91–94. doi:10.1038/nature09334
382 Chakraborty S, Doktorova M, Molugu TR, Heberle FA, Scott HL, Dzikovski B, Nagao M,
383 Stingaciu L-R, Standaert RF, Barrera FN, Katsaras J, Khelashvili G, Brown MF, Ashkar
384 R. 2020. How cholesterol stiffens unsaturated lipid membranes. *Proc Natl Acad Sci U S*
385 *A* **117**:21896–21905. doi:10.1073/pnas.2004807117
386 Connell M, Cabernard C, Ricketson D, Doe CQ, Prehoda KE. 2011. Asymmetric cortical
387 extension shifts cleavage furrow position in Drosophila neuroblasts. *Mol Biol Cell*
388 **22**:4220–4226. doi:10.1091/mbc.E11-02-0173
389 Figard L, Sokac AM. 2014. A membrane reservoir at the cell surface: unfolding the plasma
390 membrane to fuel cell shape change. *Bioarchitecture* **4**:39–46. doi:10.4161/bioa.29069
391 Figard L, Wang M, Zheng L, Golding I, Sokac AM. 2016. Membrane Supply and Demand
392 Regulates F-Actin in a Cell Surface Reservoir. *Dev Cell* **37**:267–278.
393 doi:10.1016/j.devcel.2016.04.010
394 Figard L, Xu H, Garcia HG, Golding I, Sokac AM. 2013. The plasma membrane flattens out to
395 fuel cell-surface growth during Drosophila cellularization. *Dev Cell* **27**:648–655.
396 doi:10.1016/j.devcel.2013.11.006
397 Gallaud E, Pham T, Cabernard C. 2017. Drosophila melanogaster Neuroblasts: A Model for
398 Asymmetric Stem Cell Divisions. *Results Probl Cell Differ* **61**:183–210. doi:10.1007/978-
399 3-319-53150-2_8
400 Goudarzi M, Tarbashevich K, Mildner K, Begemann I, Garcia J, Paksa A, Reichman-Fried M,
401 Mahabaleshwar H, Blaser H, Hartwig J, Zeuschner D, Galic M, Bagnat M, Betz T, Raz E.
402 2017. Bleb Expansion in Migrating Cells Depends on Supply of Membrane from Cell
403 Surface Invaginations. *Dev Cell* **43**:577-587.e5. doi:10.1016/j.devcel.2017.10.030
404 Hirani N, Illukkumbura R, Bland T, Mathonnet G, Suhner D, Reymann A-C, Goehring NW. 2019.
405 Anterior-enriched filopodia create the appearance of asymmetric membrane
406 microdomains in polarizing C. elegans zygotes. *J Cell Sci* **132**. doi:10.1242/jcs.230714

407 Ho J, Tumkaya T, Aryal S, Choi H, Claridge-Chang A. 2019. Moving beyond P values: data
408 analysis with estimation graphics. *Nat Methods* **16**:565–566. doi:10.1038/s41592-019-
409 0470-3
410 Homem CCF, Knoblich JA. 2012. Drosophila neuroblasts: a model for stem cell biology
411 **139**:4297–4310. doi:10.1242/dev.080515
412 Illukkumbura R, Bland T, Goehring NW. 2019. Patterning and polarization of cells by
413 intracellular flows. *Curr Opin Cell Biol* **62**:123–134. doi:10.1016/j.ceb.2019.10.005
414 Izumi Y, Ohta N, Itoh-Furuya A, Fuse N, Matsuzaki F. 2004. Differential functions of G protein
415 and Baz-aPKC signaling pathways in Drosophila neuroblast asymmetric division. *J Cell*
416 *Biol* **164**:729–738. doi:10.1083/jcb.200309162
417 Kabeche R, Howard L, Moseley JB. 2015. Eisosomes provide membrane reservoirs for rapid
418 expansion of the yeast plasma membrane. *J Cell Sci* **128**:4057–4062.
419 doi:10.1242/jcs.176867
420 Knoblich JA. 2010. Asymmetric cell division: recent developments and their implications for
421 tumour biology. *Nat Rev Mol Cell Biol* **11**:849–860. doi:10.1038/nrm3010
422 Knoblich JA. 2008. Mechanisms of asymmetric stem cell division. *Cell* **132**:583–597.
423 doi:10.1016/j.cell.2008.02.007
424 LaFoya B, Prehoda KE. 2021. Actin-dependent membrane polarization reveals the mechanical
425 nature of the neuroblast polarity cycle. *Cell Rep* **35**:109146.
426 doi:10.1016/j.celrep.2021.109146
427 Lang CF, Munro E. 2017. The PAR proteins: from molecular circuits to dynamic self-stabilizing
428 cell polarity. *Dev Camb Engl* **144**:3405–3416. doi:10.1242/dev.139063
429 Meenderink LM, Gaeta IM, Postema MM, Cencer CS, Chinowsky CR, Krystofiak ES, Millis BA,
430 Tyska MJ. 2019. Actin Dynamics Drive Microvillar Motility and Clustering during Brush
431 Border Assembly. *Dev Cell* **50**:545-556.e4. doi:10.1016/j.devcel.2019.07.008
432 Munro E, Nance J, Priess JR. 2004. Cortical flows powered by asymmetrical contraction
433 transport PAR proteins to establish and maintain anterior-posterior polarity in the early
434 C. elegans embryo. *Dev Cell* **7**:413–424. doi:10.1016/j.devcel.2004.08.001
435 Oon CH, Prehoda KE. 2021. Phases of cortical actomyosin dynamics coupled to the
436 neuroblast polarity cycle. *eLife* **10**:e66574. doi:10.7554/eLife.66574
437 Oon CH, Prehoda KE. 2019. Asymmetric recruitment and actin-dependent cortical flows drive
438 the neuroblast polarity cycle. *eLife* **8**. doi:10.7554/eLife.45815

439 Pang DJ, Hayday AC, Bijlmakers M-J. 2007. CD8 Raft Localization Is Induced by Its Assembly
440 into CD8αβ Heterodimers, Not CD8αα Homodimers. *J Biol Chem* **282**:13884–13894.
441 doi:10.1074/jbc.M701027200
442 Pham TT, Monnard A, Helenius J, Lund E, Lee N, Müller DJ, Cabernard C. 2019.
443 Spatiotemporally Controlled Myosin Relocalization and Internal Pressure Generate
444 Sibling Cell Size Asymmetry. *iScience* **13**:9–19. doi:10.1016/j.isci.2019.02.002
445 Ramat A, Hannaford M, Januschke J. 2017. Maintenance of Miranda Localization in Drosophila
446 Neuroblasts Involves Interaction with the Cognate mRNA. *Curr Biol CB* **27**:2101-
447 2111.e5. doi:10.1016/j.cub.2017.06.016
448 Roubinet C, Tsankova A, Pham TT, Monnard A, Caussinus E, Affolter M, Cabernard C. 2017.
449 Spatio-temporally separated cortical flows and spindle geometry establish physical
450 asymmetry in fly neural stem cells. *Nat Commun* **8**:1383. doi:10.1038/s41467-017-
451 01391-w
452 Scholze MJ, Barbieux KS, De Simone A, Boumasmoud M, Süess CCN, Wang R, Gönczy P.
453 2018. PI(4,5)P2 forms dynamic cortical structures and directs actin distribution as well
454 as polarity in Caenorhabditis elegans embryos. *Dev Camb Engl* **145**.
455 doi:10.1242/dev.164988
456 Sokac AM. 2017. Seeing a Coastline Paradox in Membrane Reservoirs. *Dev Cell* **43**:541–542.
457 doi:10.1016/j.devcel.2017.11.013
458

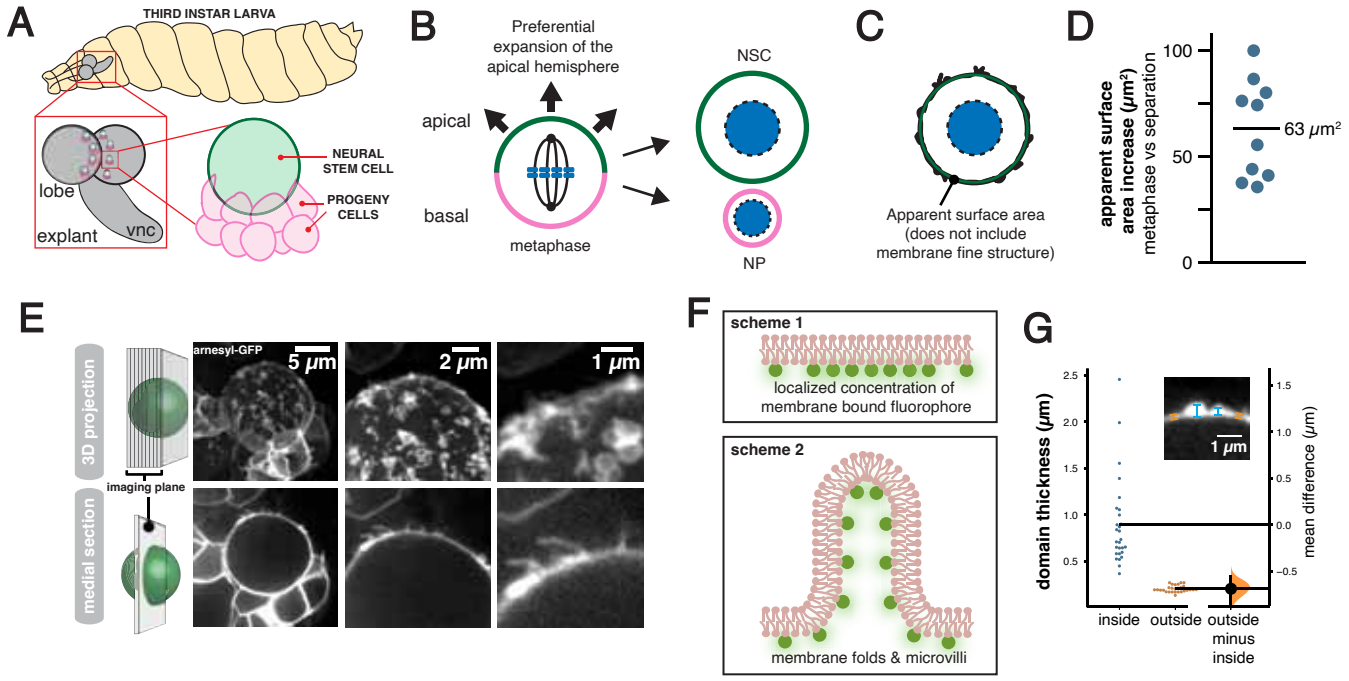

Figure 1 Neural stem cell membrane domains store excess membrane

(**A**) *Drosophila* larval central nervous system explants used in this study. Larval brain lobe neural stem cells were imaged from explants dissected from third instar larvae (vnc: ventral nerve cord).

(**B**) Model for the unequal division of neural stem cells. Preferential expansion of the apical hemisphere that occurs when the internal pressure increases during anaphase contributes to the formation of a larger apical sibling. NSC = neural stem cell. NP = neural progenitor.

(**C**) The apparent surface area of the cell follows the geometry of the main cell body and does not include the surface area contributed by the fine structure of the plasma membrane (e.g. folds and microvilli).

(**D**) Overall increase in apparent surface area that accompanies NSC division. The difference in apparent surface area at the completion of cytokinesis compared to metaphase is shown for divisions of 11 different NSCs.

(**E**) Examples of NSC membrane structure associated with localized regions of increased membrane sensor (farnesyl-GFP) intensity. A maximum intensity projection (3D projection) and medial section are shown.

(**F**) Schemes for localized enrichment of membrane sensor: 1) a configuration that yields a localized increase in sensor concentration by increased density on a single plasma membrane. 2) a configuration that yields a localized increase in intensity with uniform sensor concentration but increased membrane density.

(**G**) Variation of NSC membrane thickness associated with localized regions of increased membrane sensor intensity (membrane domains). The thickness of the membrane is shown inside and outside the domain as shown in the inset. The outside thickness is approximately equal to the diffraction limited minimum thickness.

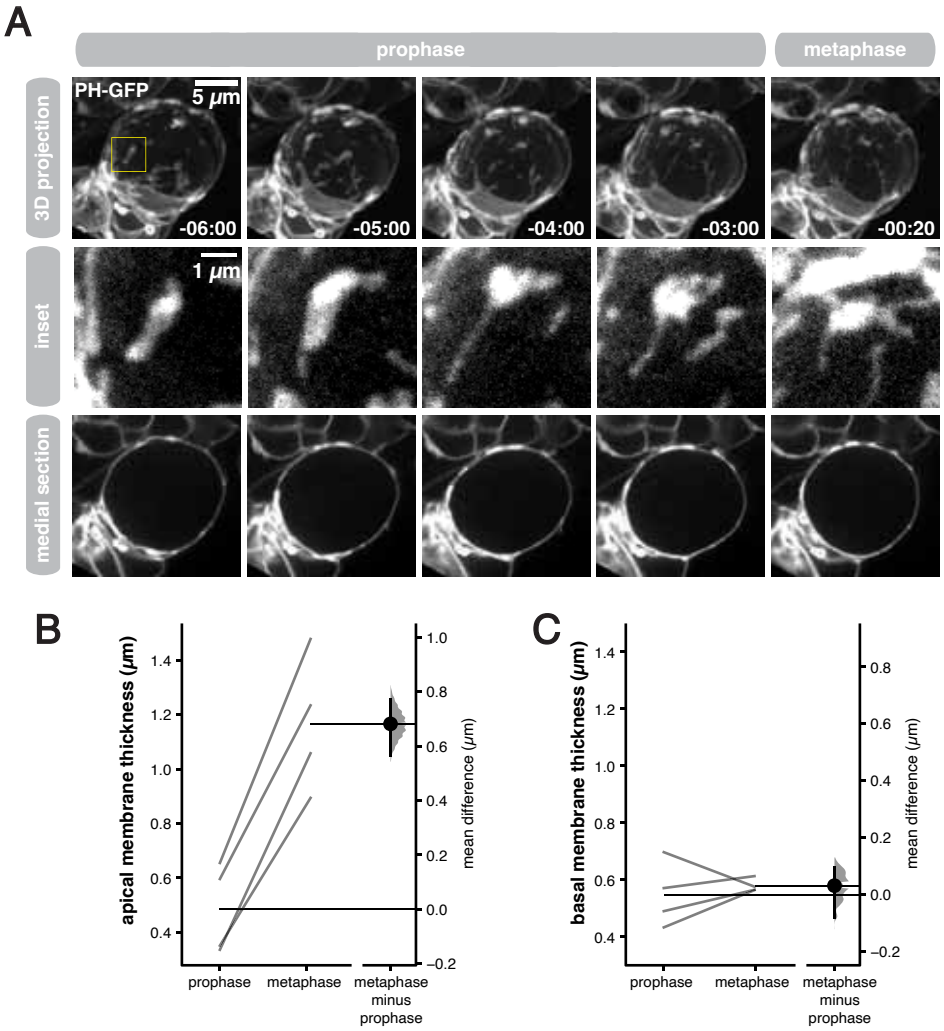

Figure 2 Apically-directed membrane domain movements during prophase form a metaphase membrane reservoir

(**A**) Frames from Video S1 showing the apically-directed movement of excess membrane during prophase that leads to the accumulation of excess membrane (worniu-GAL4>UAS-PLCd-PH-GFP; "PH-GFP") near the apical pole at metaphase. A standard deviation projection ("3D projection") is shown along with a medial section. Inset shows the basal and apical extent of one excess membrane domain as it moves apically. Time is shown relative to anaphase onset (mm:ss).

(**B**) Membrane thickness increases at the apical pole from prophase to metaphase. A paired Gardner-Altman estimation plot is shown for apical membrane thickness before apical movement commenced and metaphase. The 95% confidence interval is shown along with the bootstrap estimation distribution.

(**C**) Membrane thickness does not significantly increase at the basal pole between prophase and metaphase. Data shown as in (B).

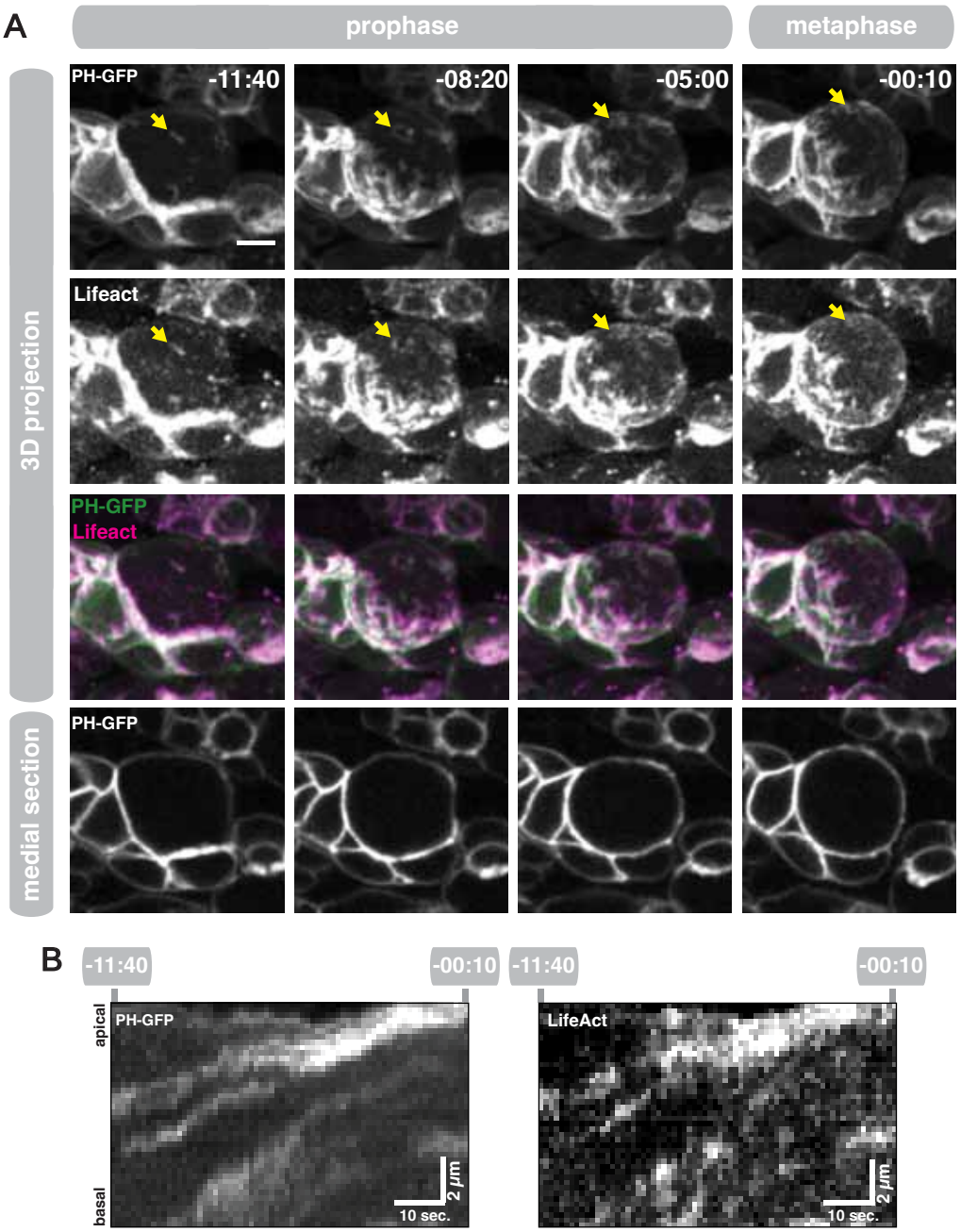

Figure 3 Apically-directed flows of actomyosin underlie the movement of excess membrane towards the apical pole

(**A**) Selected frames from Video S2 showing coordinated movement of excess membrane domains (worniu-GAL4>UAS-PLCd-PH-GFP; "PH-GFP") and cortical F-actin (worniu-GAL4>UAS-Lifeact-mRuby; "Lifeact") during prophase. A maximum intensity projection ("3D projection") is shown along with a medial section. Arrows show correlated movement of an excess membrane domain and the corresponding localized cortical actin enrichment. Time is shown relative to anaphase onset (mm:ss).

(**B**) Kymograph constructed from Video S2 of a section along the apical-basal axis showing apically-directed movements of excess membrane domains and cortical F-actin. Time is shown relative to anaphase onset (mm:ss).

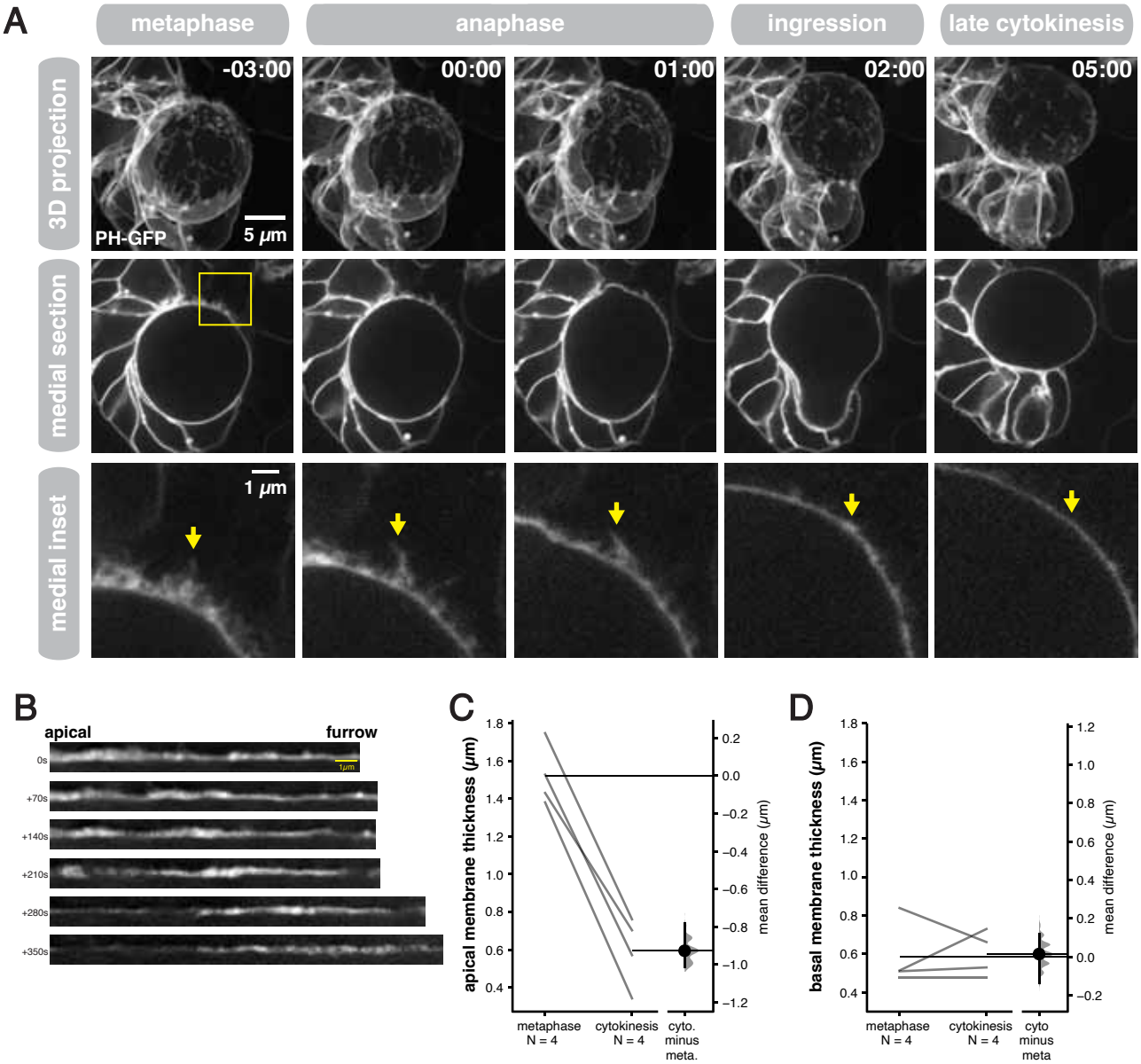

Figure 4 Consumption of the apical membrane reservoir during anaphase expansion
(**A**) Frames from Video S3 showing the consumption of the apical membrane reservoir through anaphase, furrow ingression, and late cytokinesis. Box shows inset area in row 3. A standard deviation projection (”3D projection”) is shown of the membrane (wor-niu-GAL4>UAS-PLCd-PH-GFP; “PH-GFP”) along with a medial section. Arrows show microvilli as it is absorbed into the cell body. Time is shown relative to anaphase onset (mm:ss).
(**B**) Straightened membrane sections from Video S3 showing the apical pole to the furrow at times relative to anaphase onset.
(**C**) Membrane thickness at the apical pole at metaphase and the completion of cytokinesis. A paired Gardner-Altman estimation plot is shown for apical membrane thickness at both time points. The 95% confidence interval is shown along with the bootstrap estimation distribution.
(**D**) Membrane thickness at the basal pole at metaphase and the completion of cytokinesis. Data is shown as in (C) but for the membrane near the basal pole.

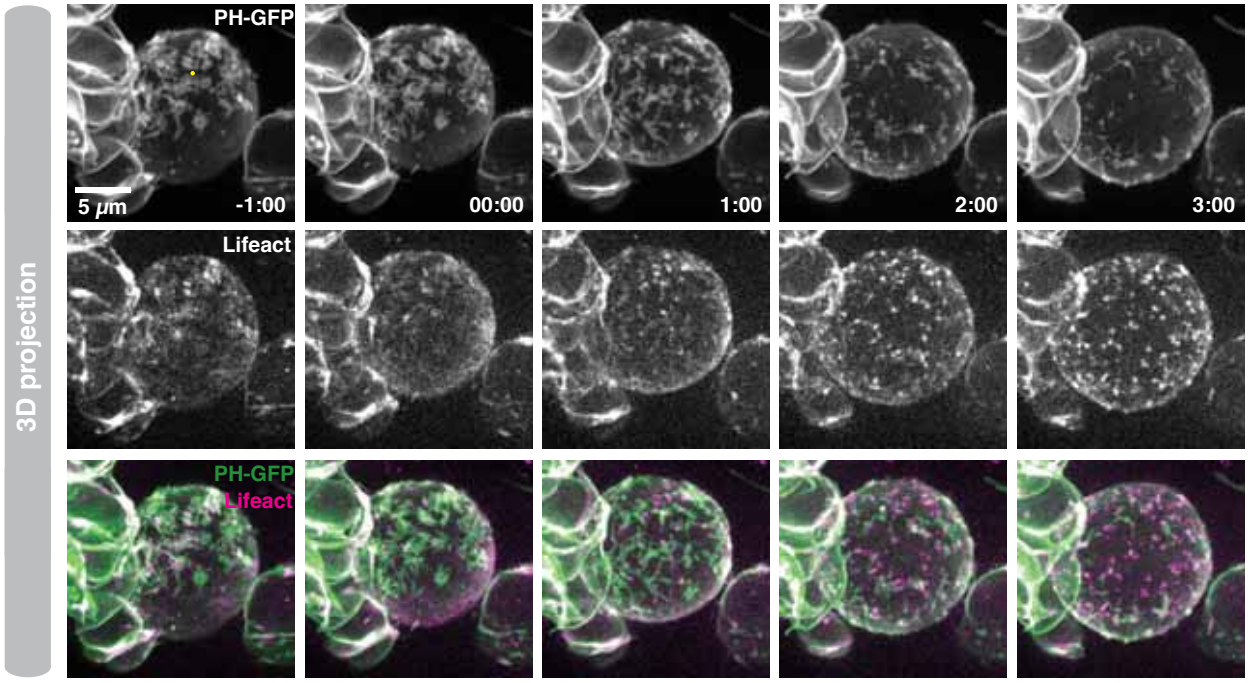

Figure 5 Cortical actin dynamics during membrane reservoir consumption
Selected frames from Video S5 showing correlated F-actin and membrane dynamics (worniu-GAL4>UAS-PLCd-PH-GFP; “PH-GFP”) and cortical F-actin (worniu-GAL4>UAS-LifeAct-mRuby; ”Lifeact”) during anaphase. Standard deviation projection view of the apical hemisphere (apical pole is marked with a yellow circle). Time is shown relative to anaphase onset (mm:ss).

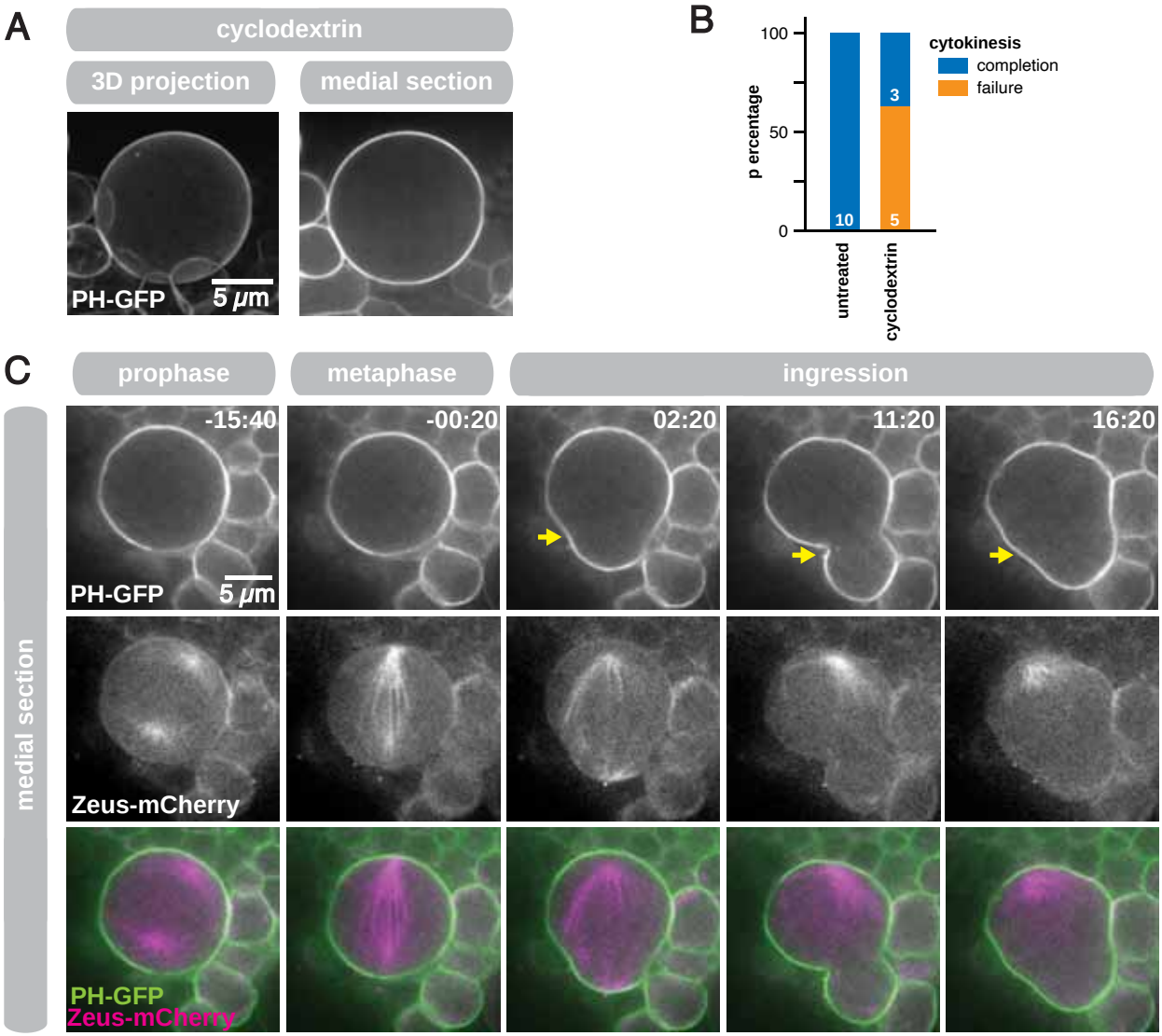

Figure 6 Cyclodextrin treatment removes excess membrane
(**A**) Standard deviation projection (”3D projection”) and medial section showing the effect of cyclodextrin treatment on the NSC membrane (worniu-GAL4>UAS-PLCd-PH-GFP; “PH-GFP”).
(**B**) Effect of cyclodextrin treatment on cytokinesis. “Completion” denotes cells that completed furrowing whereas “failure” denotes cells whose furrow failed to completely close.
(**C**) Selected frames from Video S6 showing the effect of cyclodextrin treatment on the NSC membrane and NSC cytokinesis. Arrows mark furrow that initially ingresses and ultimately retracts. The Zeus-mCherry microtubule binding protein is shown in the second row and merge. Time is shown relative to anaphase onset (mm:ss).

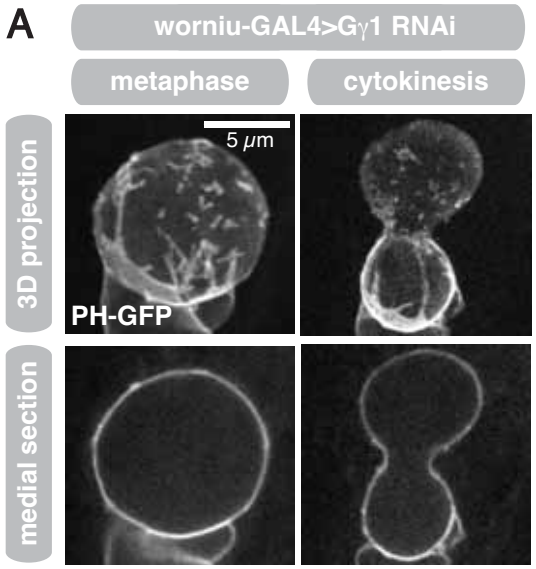

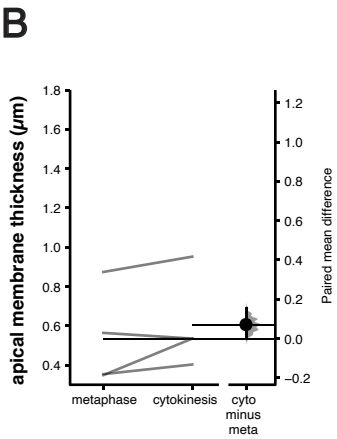

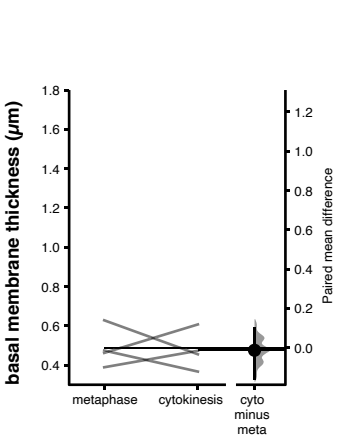

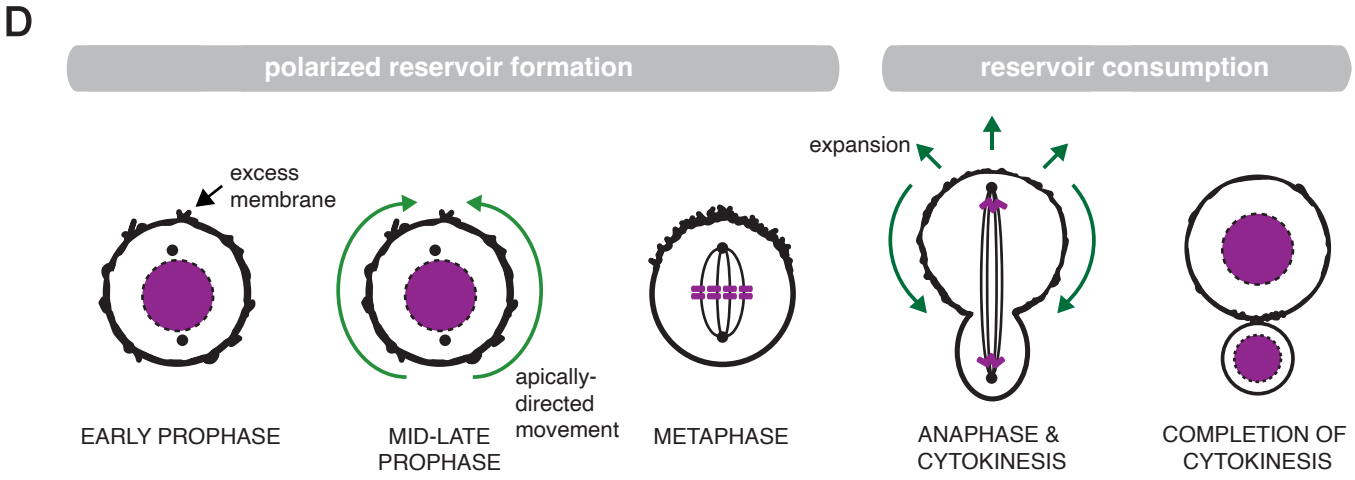

Figure 7 Membrane reservoir asymmetry is required for biased expansion
(**A**) Selected frames from Video S7 of an NSC expressing RNAi directed against Gγi. A standard deviation projection ("3D projection") is shown of the membrane (worniu-GAL4>UAS-PLCd-PH-GFP; "PH-GFP") along with a medial section.
(**B**) Membrane thickness at the apical pole at metaphase and the completion of cytokinesis for Gγi-expressing NSCs. A paired Gardner-Altman estimation plot is shown for apical membrane thickness at both time points. The 95% confidence interval is shown along with the bootstrap estimation distribution.
(**C**) Membrane thickness at the basal pole at metaphase and the completion of cytokinesis. Data is shown as in (B) but for the membrane near the basal pole.